Lineal energy calibration of a mini-TEPC via the proton-edge technique

A. Bianchi[a,b,c], D. Mazzucconi[c,d], A. Selva[c], P. Colautti[c], A. Parisi[a], F. Vanhavere[a], B. Reniers [b], V. Conte[c]

[a] *Belgian Nuclear Research Centre SCK CEN, Boeretang 200, 2400 Mol, Belgium*
[b] *University of Hasselt, Faculty of Engineering Technology, Centre for Environmental Sciences, Nuclear Technology Center, Agoralaan, 3590 Diepenbeek, Belgium*
[c] *Istituto Nazionale di Fisica Nucleare INFN, Laboratori Nazionali di Legnaro, viale dell'Università 2, Legnaro (Padova), Italy*
[d] *Politecnico di Milano, Dipartimento di Energia, via La Masa 34, Milano, Italy*
Corresponding author: Bianchi Anna – anna.bianchi@sckcen.be

Short running title:

Proton-edge calibration of a mini-TEPC

Keywords: Microdosimetry, mini-TEPC, calibration, Proton Therapy

Abstract

Purpose: The possibility to calibrate microdosimetric spectra using the proton- and electron-edge was proposed many years ago. It consists of two steps: first identifying the edge and a marker point on it and then ascribing the correct lineal energy value to the position of the edge in the event size spectrum. The purpose of this work is to rigorously study the marker identification for the proton-edge in the mini-TEPC spectra measured in neutron and in clinical proton fields, and the correspondent lineal energy value to assign to it.

Materials and Methods: Microdosimetric measurements were performed with a cylindrical miniaturized tissue-equivalent proportional-counter (mini-TEPC) in neutron and gamma rays radiation fields at the CN accelerator of the Legnaro National Laboratories of the Italian National Institute for Nuclear Physics (LNL-INFN) and in the clinical 62 MeV proton beam of the Southern National Laboratories of INFN (LNS-INFN). The fitting of the proton-edge region of the microdosimetric spectra with a Fermi-like function was studied in both neutron and proton fields to identify the most precise marker point. The lineal energy value to ascribe to it was determined starting from the maximum energy deposit in protons obtained in FLUKA simulations.

Results: Both in neutron radiation field and in clinical proton beams the flex and the intercept of the tangent through the inflection point are determined with similar precision. The flex was chosen as the most suitable marker of the proton-edge in sealed detectors because it is known to be less sensitive to pressure variations. The lineal energy value to ascribe to the flex position for 0.75 µm of propane depends on the irradiation geometry: 194 keV/µm for isotropic radiation fields and 165 keV/µm for mono-directional radiation fields orthogonal to the axis of the cylinder. The calibration values for the proton-edge have been converted in water by means of the mean stopping power ratio of water and propane for protons obtaining 171 keV/µm for isotropic radiation fields and 145 keV/µm for mono-directional radiation fields.

1. Introduction

The stochastics of the energy deposition process at the micrometre level is an important feature of the radiation field that can be related to its biological effect on cells [Wambersie et al., 1990; Menzel et al., 1990]. Based on that, microdosimetry aims at measuring the energy deposited by single events in target sites of micrometre size. The reference detector is the tissue-equivalent proportional counter (TEPC), a gas proportional counter typically of spherical or cylindrical shape, constructed with materials having approximately the same chemical composition of biological tissue. The filling gas is also almost tissue equivalent, and based on the density scaling principle, micrometre site sizes are simulated with cavities of the millimetre or centimetre scale.

In order to avoid pile up effects, the maximum typical counting rate which can be sustained by TEPCs and associated electronics is in the range $5\text{-}50 \cdot 10^3$ counts per second. However, the usual counting rate in proton therapy beams is generally much higher, even at the minimum sustainable beam current, unless the cross sectional area of the detector is reduced to less than 1 mm^2. Therefore, miniaturized TEPCs (mini-TEPC) with a sensitive volume of 0.9 mm in diameter have been developed at the Legnaro National Laboratories of the Italian National Institute for Nuclear Physics (LNL-INFN) for specific application in particle radiation therapy [De Nardo et al., 2004]. The first mini-TEPCs worked with a continuous gas flow to prevent gas gain instabilities due to outgassing phenomena. However, the gas flowing system discourages the use of mini-TEPCs in clinical environment due to Fire Safety Policy and procedures. Therefore, a new prototype detector able to work with good reproducibility without gas flow [Conte et al., 2019] has been designed, constructed and assembled.

The fundamental microdosimetric quantity is the lineal energy, which is defined as the ratio of the random variable energy imparted to the mass in the sensitive volume (SV) and the mean chord length in that volume for randomly oriented chords (μ-randomness). However, TEPCs really measure the number of ion pairs produced in the SV, and this number is later converted to energy deposit by means of the W-value, the mean energy expended by incoming radiation per ion pair formed, provided that the average gas-gain is known. More frequently, the pulse height distribution measured at the output of a charge sensitive preamplifier is directly calibrated in terms of lineal energy, by using one of a few different calibration methods reported in literature [Lindborg L. et al., 2017]. In the past, the most common method consisted of using a reference calibration alpha source of well-known energy. The energy lost by the alpha particle crossing the SV can be calculated with range-energy data tables for the selected gas.

Since miniaturized TEPCs cannot be supplied with an internal calibration source due to limited space available, alternative calibration procedures must be applied. This paper reports on the study of the intrinsic calibration technique that exploits the feature of the proton-edge (p-edge). This procedure consists in determining a marker point in the characteristic proton-edge region of microdosimetric spectra to the position of which a specific lineal energy value is assigned. The proton-edge calibration technique was proposed many years ago, here the consistency with other calibration techniques was analysed, including a detailed discussion on the uncertainty budget.

Specifying the different contributions allows to understand which procedures can be improved in order to reduce the overall uncertainty.

2. Material and Methods

2.1 The mini-TEPC

The mini-TEPC developed at LNL-INFN [De Nardo et al., 2004], was recently upgraded to work without gas flow [Conte et al., 2019]. In particular, the gas ducts were enlarged in order to facilitate the cleaning, outgassing and filling procedure of the detector. Moreover, more attention was paid to vacuum tightness during the machining and assembly of all the components.

The sensitive volume is a cylinder of 0.9 mm in diameter and height surrounded by a 0.35 mm thick A150 plastic wall that works as cathode. The anode is a 10 µm golden-plated tungsten wire. The A150 cylinder is surrounded by a 0.35 mm thick insulating shell of Rexolite®. The whole detector is inserted in a 0.2 mm thick titanium sleeve, for an overall external diameter of 2.7 mm (see Figure 1). The total water equivalent thickness of the detector walls, based on the ratio of the stopping powers in the different materials, was calculated as 1.37 mm [Conte et al., 2019].

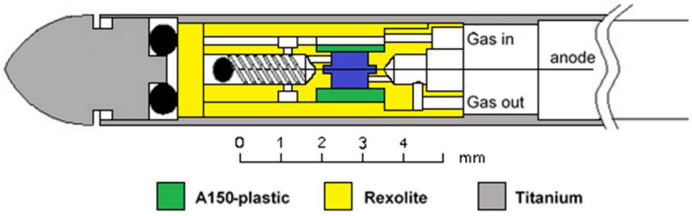

Figure 1 – Section of the new mini-TEPC

The detector was filled with pure propane gas at a pressure of 45.4 kPa, corresponding to a site size of 0.75 µm when scaled at density 1 g/cm³. The reason behind this choice of gas pressure is based on a previous work [Chiriotti et al., 2015], showing that the frequency distribution of ionizations measured in a volume filled with propane-based tissue-equivalent gas mixture at 1 µm simulated diameter is well reproduced by the corresponding distribution measured with pure propane if the gas pressure is reduced to simulate a site size of 0.75 µm at unit density. Since 1 µm is a standard tissue equivalent site size, using propane gas at this pressure allows to get spectral distributions of lineal energy that are comparable with those in literature measured in tissue equivalent gases. The gas pressure was continuously monitored by means of an absolute pressure transducer MKS Baratron type 722A. One year after sealing the gas pressure varied by less than 2%.

The detector is equipped with a customized low noise charge-sensitive preamplifier having a dynamic range of more than 4 orders of magnitude. Signals from the output of the preamplifier were then fed to two linear pulse-shaping amplifiers operated in parallel, with gain settings in the ratio 10:1. A shaping time of 0.5 µs was used for this work. The Gaussian-shaped pulses were then digitized by a 14-bit ORTEC Model AD114 and a 13-bit ORTEC Model AD413 CAMAC-ADCs,

and finally stored in an ORTEC HM413 histogramming memory. The two sub-spectra were joined offline by matching the overlapping event-size regions.

2.2 The measurements

In order to get a clear p-edge, microdosimetric spectra were measured in the low energy neutron radiation field produced with the reaction $^{7}Li(p,n)^{7}Be$ at the CN accelerator of LNL-INFN using a 2.4 MeV proton beam impinging continuously on a 100 μm thick ^{7}Li target. The Q-value of the reaction is Q = - 1.644 MeV and the threshold is 1.880 MeV, the maximum neutron energy is 0.52 MeV. The target used in this measurement campaign is a pure ^{7}Li target 100 μm thick deposited on a semi-spherical copper layer, the system is air-cooled. The radiation field was considered isotropic. The detector was positioned vertically at 0.5 cm from the target.

The second measurement campaign was performed at the clinical 62 MeV proton beam of CATANA at the LNS-INFN [Cirrone et al., 2004], which is used to treat ocular melanoma. A half-modulated Spread Out Bragg Peak (SOBP) was used, with a total range in water of 2.9 cm and a modulation width of 1.1 cm. Ten spectra were acquired across the SOBP interposing calibrated layers of PMMA between the collimator and the detector. The measurement positions along the dose profile are shown in Figure 2.

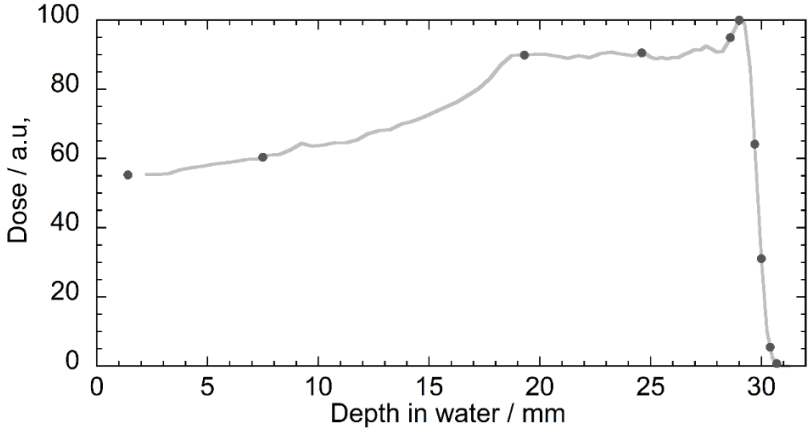

Figure 2 – Dose profile (solid line) and measurement positions (dots).

All the measurements were performed biasing the detector cathode at – 700 V and keeping the anode grounded through the preamplifier. The lowest detection threshold at the CN accelerator was 1 keV/μm due to the high background electronic noise present in the experimental room while it was around 0.5 keV/μm for the measurements acquired at CATANA.

2.2 The FLUKA simulations

In order determine the lineal energy value at the proton-edge, the response of the mini-TEPC was simulated by means of the Monte Carlo code FLUKA [Böhlen et al., 2014; Ferrari et al., 2005]. A simplified geometry of the TEPC was reproduced in FLUKA neglecting all the cavities present in the real detector for electrical connections and gas circulation. The 0.9 mm sensitive volume is surrounded by the A-150 cathode (0.35 mm thick), then by the solid Rexolite insulating shell

(0.35 mm thick) and finally by the 0.2 mm thick titanium sleeve. The cavity was filled with propane gas at 45.4 kPa, corresponding to a site size of 0.75 μm when scaled at density 1 g/cm³.
To achieve the best accuracy in the Monte Carlo transport, the electrons, gamma rays and protons thresholds were set to 1 keV (i.e. the minimum energy cut-off which can be set in this code) in the sensitive volume and also in all the surrounding regions (e.g. cathode wall, anode, Rexolite).
The distribution of the energy deposited in the sensitive volume of the mini-TEPC was simulated in the gamma rays radiation field produced by a ^{137}Cs source, the neutron field from the ^{7}Li(p,n)^{7}Be reaction and the proton SOBP of CATANA.
The experimental SOBP of CATANA is obtained by modulating the accelerated beam through the modulation wheel. In order to produce a uniform transverse profile, the wheel is kept in rotation during the irradiation. This configuration is not actually reproducible with the FLUKA code, since the simulation of moving objects is not yet implemented. The modulating system was substituted with a fictitious proton source characterized by an energy distribution equivalent to that of the beam downstream of the rotating device. This energy distribution was calculated by irradiating a steady wheel in different positions. FLUKA simulations were also exploited for assessing the probability distributions of the track lengths described by the particles traversing the sensitive region [Mazzucconi et al., 2018].

3. Lineal energy calibration: the selection of the marker point

3.1 Selection of a marker point in neutron spectra

The intrinsic lineal energy calibration based on the p-edge technique consists in determining a marker point in the characteristic proton-edge region of the microdosimetric spectra, which represents the maximum energy that can be deposited, in neutron a radiation field, by a recoil proton in the sensitive volume and then assigning a specific lineal energy value to its position.
To give an example of a typical neutron microdosimetric spectrum as a function of the pulse height h prior to the lineal energy calibration, Figure 3 shows the frequency probability density $f(h)$, and the frequency and dose distributions $hf(h)$ and $hd(h)$. In the $hf(h)$ vs. $\log(h)$ representation (frequency distribution), equal areas under the curve represent equal fractions of the total number of events. In the $hd(h)$ vs. $\log(h)$ representation (dose distribution), equal areas under the curve represent equal fractional doses. The p-edge region, highlighted as a grey zone in Figure 3, is the sharp drop-off region that is recognizable in the $f(h)$ distribution only if plotted in double log scale (right panel of Figure 3) but becomes evident in the $hf(h)$ curve and even more in the $hd(h)$ distribution. Due to energy straggling, this region has a typical reverse sigmoidal shape.

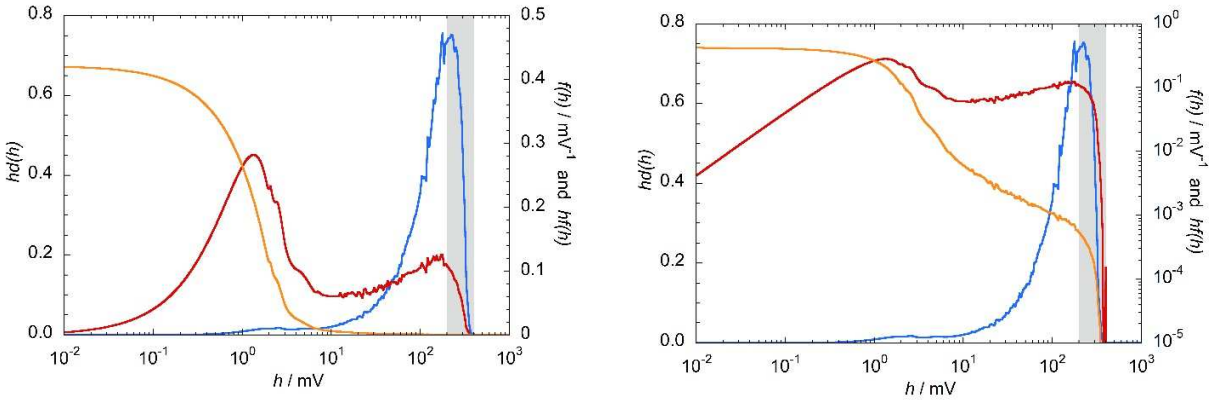

Figure 3 – *f(h)* in orange, *hf(h)* in red and *hd(h)* distribution in blue. On the left they are plotted in semi-logarithmic representation and on the right *f(h)* and *hf(h)* are plotted in double logarithmic representation.

Following the procedure recommended by [Conte et al., 2013] for the electron-edge, the proton-edge was fitted with a Fermi-like function: $h \cdot d(h) = \frac{A}{1+exp^{B(h-C)}}$ (1)

where ***C*** has the same dimension as *h*, and ***B*** the dimension of the reciprocal of *h*. ***A*** is the upper asymptote of the function; ***B*** is inversely related to the steepness of the function around the inflection point and ***C*** is the position of the inflection point at which $h \cdot d(h) = A/2$.

Two positions were considered as suitable marker points: the position of the inflection point h_{flex}, and the position h_{tC} of the intercept of the tangent through the inflection point with the *h*-axis. For a Fermi-like function the marker points are described by simple analytical expressions of the function parameters ***B*** and ***C***: $h_{flex} = C;\ h_{tC} = \frac{2}{B} + C$ (2)

The neutron spectrum used in the analysis is plotted in Figure 4.

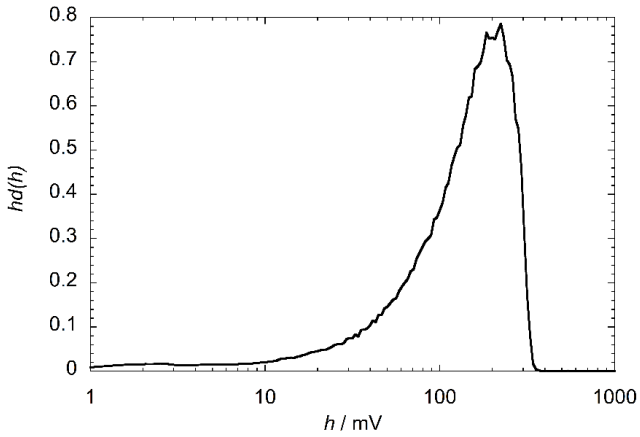

Figure 4 – Spectrum acquired in neutron radiation field.

The first step is the analysis on the precision of the marker point determination with the fitting procedure, which is applied to the experimental data, binned at 600 points per decade.

The choice of the width of the fitting region is somehow arbitrary, therefore the effect of different choices was investigated. Fifteen different fitting procedures were applied, corresponding to 15 different selections of the fitting region. The width of the region was changed by changing the lower fitting boundary, while the higher boundary was kept the same as it plays only a minor role. The fitting functions obtained by fitting the data of Figure 4 with three different lower boundaries, the two at the extreme positions and one in the middle, are shown in Figure 5.

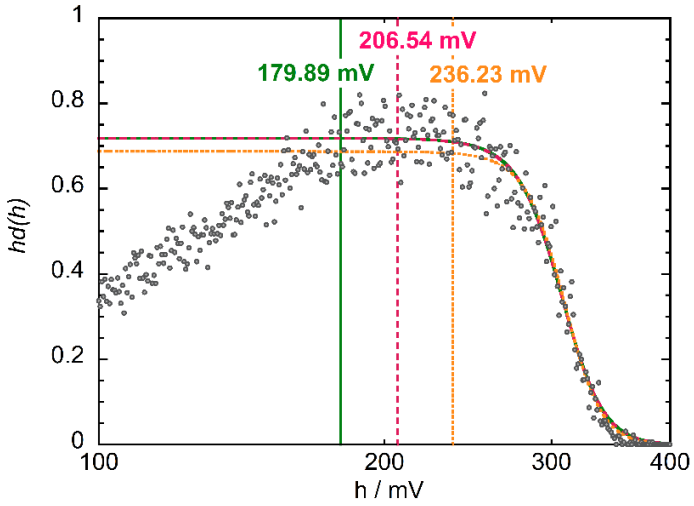

Figure 5 – Neutron spectrum binned at 600 bin/decade fitted with three different lower boundaries.

The whole set of values for h_{flex}, and the h_{tC} resulting from the fifteen different fits are listed in Table 1. All the uncertainties refer to one standard deviation. . The relative standard deviation in the data set is always below 0.25% for h_{flex} and below 0.12% for h_{tC}.

Lower fitting boundary / mV	$\boldsymbol{h_{flex}}$ / mV	$\boldsymbol{h_{tC}}$ / mV
179.89	306.5 ± 0.7	338.5 ± 0.4
184.08	306.5 ± 0.7	338.5 ± 0.4
187.64	306.4 ± 0.7	338.6 ± 0.4
191.28	306.6 ± 0.7	338.5 ± 0.4
194.98	306.6 ± 0.7	338.5 ± 0.4
198.76	306.4 ± 0.7	338.6 ± 0.4
202.61	306.7 ± 0.7	338.4 ± 0.4
206.54	306.5 ± 0.7	338.5 ± 0.4
210.54	306.6 ± 0.7	338.5 ± 0.4
214.62	307.0 ± 0.7	338.2 ± 0.4
218.78	307.0 ± 0.7	338.2 ± 0.4
223.01	307.5 ± 0.7	338.0 ± 0.4
227.34	308.0 ± 0.7	337.7 ± 0.4
231.74	308.2 ± 0.7	337.6 ± 0.4
236.23	308.7 ± 0.7	337.4 ± 0.4
Average	**307.0 ± 0.2**	**338.2± 0.1**

Table 1 – Fitting results of the p-edge in raw spectra in neutron radiation field with different lower boundaries

It should be observed (Table 1) that for both markers uncertainties are smaller than 0.5%, being the intercept slightly more precise.

To continue the study on the precision of the markers in the p-edge region, the fitting procedure was analysed for the same spectrum, but acquired with different statistics. The spectrum considered for Table 1 had an overall statistic of 10^6 events, where the number of events above the lowest fitting boundary was about 10^5, representing the 10% of the total number of events.

However, it may happen that the number of measured events in the proton-edge region is lower and therefore, the next step was to study the influence of the number of events in the fitting region on the fitting markers. Two spectra acquired with a high and low statistics are plotted in Figure 6 together with the Fermi-like function fitting the proton-edge.

The spectrum with low statistics has an overall number of events equal to $3 \cdot 10^5$, while the number of events above the fitting lower boundary is $1.6 \cdot 10^4$. On the other hand, the one with high statistics, used for the boundary analysis, has an overall number of events 10 times higher than the one with low statistic and consequently the number of events above the threshold is ten times higher.

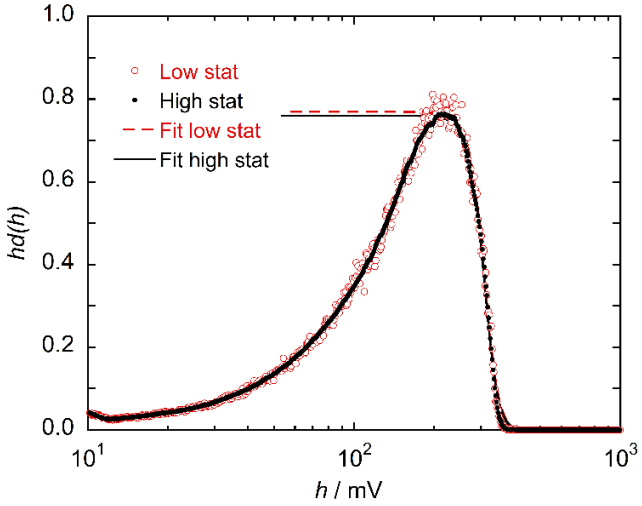

Figure 6 – Low and high statistic spectra and their Fermi-like function.

The markers of the fits are reported in Table 2, together with the maximum semi-dispersion, the marker that is less influenced by statistics is the flex ***C*** but both markers have a comparable precision.

Spectra	h_{flex} / mV	h_{tc} / mV
Low statistic	307.0 ± 0.3	344.3 ± 0.9
High statistic	306.6 ± 0.3	343.0 ± 0.9
Maximum semi-dispersion	**0.2**	**0.6**

Table 2 – Fitting markers at different statistics and maximum semi-dispersion for the two possible marker points.

By propagating the two maximum uncertainties reported in Table 1 and Table 2, the overall uncertainty on h_{flex} is 0.4% and that on h_{tC} is 0.3%.

3.2 Selection of a marker point in proton spectra

The same analysis performed in the previous paragraphs was also done for microdosimetric spectra measured in the therapeutic proton beam of CATANA. Figure 8 shows ten different *hd(h)* distributions measured across the SOBP; the measuring positions are also indicated in the figure as coloured dots in the depth-dose profile measured with a Markus ionization chamber.

The proton-edge starts being recognizable at the Bragg peak, and it is most evident at the last position, corresponding to a depth in water of 30.7 mm. The last spectrum was chosen to perform the analysis of the lineal energy calibration procedure: in this case, the percentage of events in the region of the p-edge is higher with respect to the total amount of counts and for this reason the uncertainty due to the statistics is reduced.

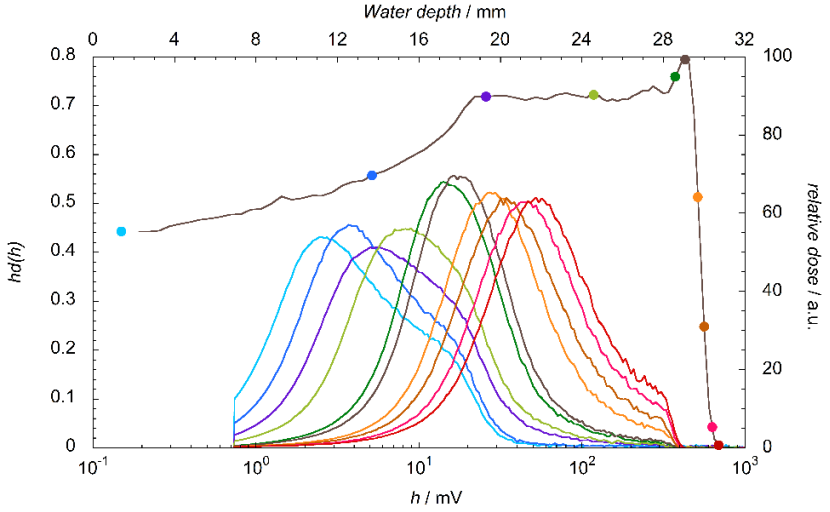

Figure 7 – Ten spectra before the lineal energy calibration and extrapolation. Coloured dots are also plotted in the depth-dose profile at the corresponding measurement position

As for the neutron field, the variability of the markers with respect to the fitting intervals was investigated: the fitting procedure was repeated 15 times by choosing different lower boundaries of the p-edge region.

The spectrum at 30.7 mm in depth is shown in Figure 8 together with three fitting boundaries (first, intermediate and last) and the Fermi-like function obtained in these intervals, extrapolated to lower *h* values, below the lower boundaries.

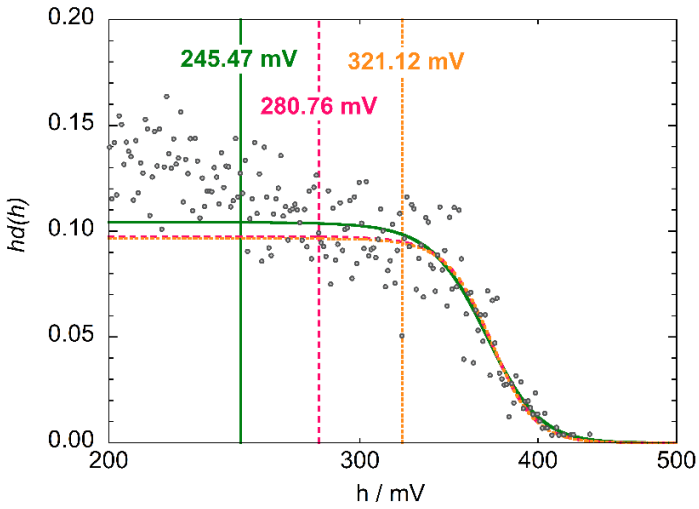

Figure 8 – Spectrum at 30.7 mm fitted with three different lower boundaries.

Differences in the flex and the intercept positions are hardly visible in this figure, therefore the complete set of numerical results from this study are listed in Table 3. All the uncertainties refer to one standard deviation.

Lower fitting boundary / mV	h_{flex} / mV	h_{tC} / mV
245.47	367 ± 1	399.6 ± 0.8
250.23	368 ± 1	398.9 ± 0.8
255.07	368 ± 1	398.8 ± 0.8
260.02	368 ± 1	398.7 ± 0.8
265.06	369 ± 1	398.3 ± 0.8
270.19	369 ± 1	398.0 ± 0.8
275.42	370 ± 1	397.8 ± 0.8
280.76	370 ± 1	397.4 ± 0.8
286.20	370 ± 1	397.3 ± 0.8
291.74	370 ± 1	397.4 ± 0.8
297.39	370 ± 1	397.4 ± 0.8
303.16	371 ± 1	397.1 ± 0.8
309.03	371 ± 1	397.0 ± 0.8
315.02	371 ± 1	397.0 ± 0.8
321.12	371 ± 1	397.1 ± 0.8
Average	**369.6 ± 0.3**	**397.8± 0.2**

Table 3 – Fitting results of the p-edge the spectrum at the end of the CATANA proton SOBP (depth of 30.7 mm) with different lower boundaries.

A summary of the study for neutron and therapeutic proton beam is shown in Figure 9. Again, as in neutron field, the marker that is slightly less influenced by the choice of the fitting range is the h_{tC}, both markers having a maximum uncertainty lower than 0.5%. Gradient colour corresponds to increasing occurrences from n=1 to n=6.

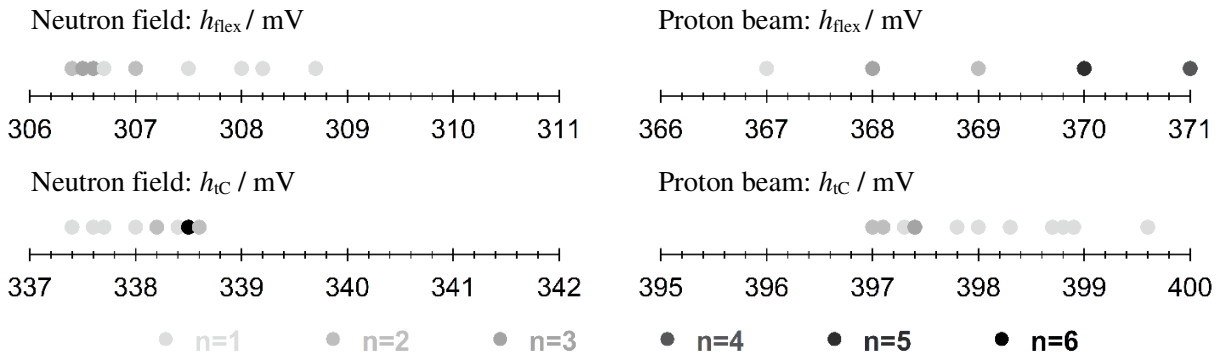

Figure 9 – Graphic representation of the values found for the flex position and the intercept in both radiation fields.

The analysis on the different statistics was performed on the last four spectra, for which the total amount of events in the p-edge region varied from 700 to 2000. An overview of the number of events in the fitting regions and their percentage on the overall statistics is reported in Table 4, these conditions guarantee that the standard deviation of the flex on the single fit (including fitting boundary and statistics) is smaller than 1%.

Depth / mm	Overall statistic	Number of events in the p-edge region (> 297.4 mV)	Fraction of events in the p-edge with respect to the total number
29.7	$2 \cdot 10^6$ events	700 events	0.035
30.0	$1.6 \cdot 10^6$ events	1100 events	0.069
30.4	$0.8 \cdot 10^6$ events	870 events	0.109
30.7	$1.1 \cdot 10^6$ events	2000 events	0.182

Table 4 – Information on the statistics of the microdosimetric spectra used for proton-edge calibration.

Figure 10 shows a detailed view of the proton edge of the different spectra fitted with the Fermi-like function at the intermediate boundary with a high-density logarithmic re-binning, i.e 600 bin/decade. The position of the flex is also reported and represented by the grey dashed line.

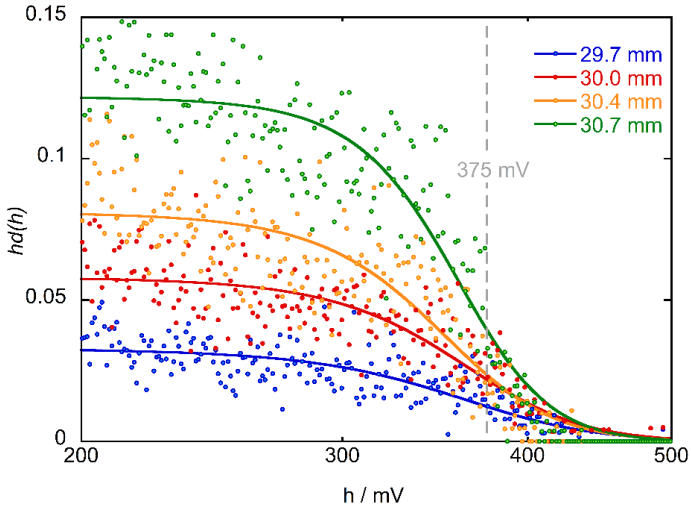

Figure 10 – Zoom of the fitting of the proton edge at the four different depths along the CATANA SOBP.

The results of the fitting procedure are given in Table 5. The relative maximum uncertainty on h_{flex} is 2.5% and that on h_{tC} is 3.2%. All uncertainties refer to one standard deviation. The overall uncertainty is higher than the values found for neutrons because the analysis have been performed in different spectra and a higher variability may occur.
By propagating the two maximum uncertainties reported in Table 3 and Table 5, the overall uncertainty on h_{flex} is 1.9% and that on h_{tC} is 3.3%.

Lower boundary	**Spectra**	h_{flex} / mV	h_{tc} / mV
297.39 mV	29.7 mm	385 ± 9	421 ± 12
	30.0 mm	379 ± 9	418 ± 12
	30.4 mm	366 ± 9	395 ± 12
	30.7 mm	370 ± 9	397 ± 12
	Average	**375 ± 5**	**408 ± 6**

Table 5 – Fitting results in different position of the proton SOBP.

3.3 Assignment of a y-value to the p-edge marker point

The next step is to assign to the most suitable marker the right value in lineal energy in order to convert the *h* vs. *hd(h)* spectrum in *y* vs. *yd(y)* spectrum.

3.3.2 Energy deposition spectra in 0.75 µm of propane

The lineal energy value that has to be assigned to the flex position can be calculated starting from the maximum energy deposit in the sensitive volume. The energy deposit by a proton is maximum when its stopping power is close to the maximum and the proton travels along the maximum chord length, which for a right circular cylinder is $D\sqrt{2}$. However, considering that the chord length distribution is peaked at the diameter, also in the case of randomly oriented chords, it is expected that the main contribution to the proton edge is due to energy deposited along the diameter, while slightly shorter and longer path lengths are partially responsible for the width of the proton edge region.
The lineal energy value at the proton edge has been evaluated with the FLUKA Monte Carlo simulations. Figure 11 shows the dose-distributions of the energy deposit $\varepsilon d(\varepsilon)$ simulated both for the neutron radiation field and for the modulated proton beam at 30.7 mm in water depth. The proton distribution is normalized to unit dose, while the neutron distribution is scaled by a constant factor to overlap the proton edge regions of the two spectra. It is possible to observe that the maximum energy deposit evaluated at the flex position of the fitted Fermi function is 97 keV, the same in both radiation fields within the statistical uncertainties.

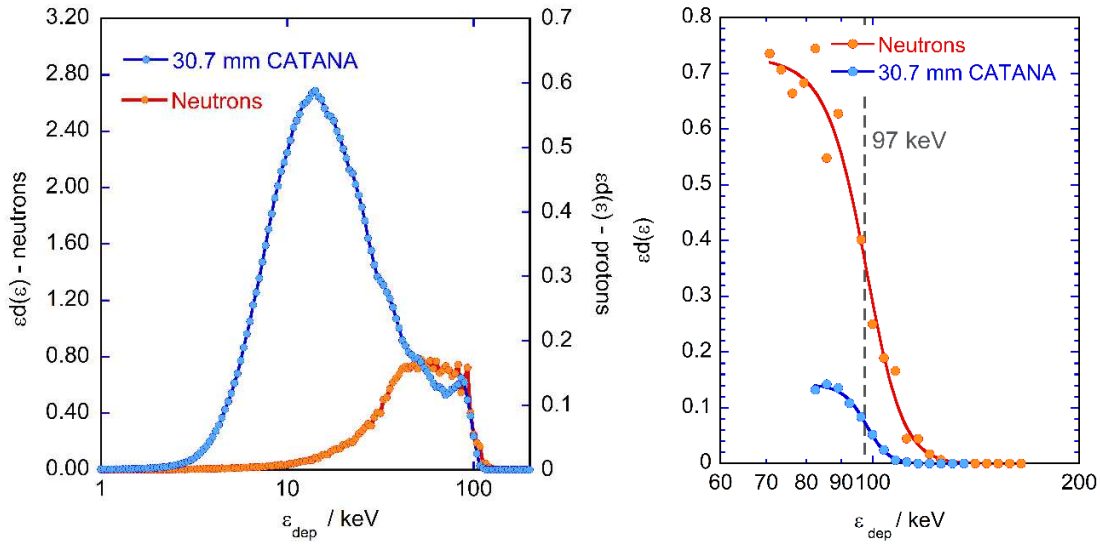

Figure 11 – Simulated energy deposit spectra (left) and a zoom in the p-edge region with the Fermi-like fit (right).

This value is the same as the result obtained by using the SRIM energy-range tables and calculating the maximum energy deposited in a 0.75 µm thickness of propane gas at density 1 g/cm^3 [Bianchi et al., 2020]. The use of different energy range tables, such as the PSTAR database from NIST [Berger et al., 2017] or the ICRU Report 49 [ICRU 49, 1993], leads to values of 92 keV and 91 keV, respectively about 7% lower. This difference in the calibration related to the input database has been already analysed and discussed in [Chiriotti et al., 2015b], the reported results underlined an uncertainty of 4% on the $y_{\text{p-edge}}$ due to the choice of the database and the final lineal energy value assigned to the marker.

3.3.2.1 From energy deposit to lineal energy

ICRU 36 [ICRU 36, 1983] and ICRU 85 [ICRU 85, 2011] define the lineal energy y as the ratio between the energy imparted by a single energy-deposition event and the mean chord length of the irradiated volume. The mean chord length is calculated for isotropic uniform random chords (µ-randomness). According to the Cauchy's formula, for a convex body of any shape $\bar{l}_{\mu} = 4V/S$, being V and S the volume and surface of the body, respectively. For a right cylinder with equal height H and diameter D, the average chord length is $\bar{l}_{\mu} = (2/3)D$, that is 0.5 µm, considering a site size of 0.75 µm of propane.

However, when a cylindrical volume is irradiated by a parallel beam orthogonal to its main axis, the distribution of the path lengths of protons intersecting the volume differs from the chord length distribution for randomly oriented chords. The mean value of this distribution, the mean path length, is $\bar{l}_{\text{path}} = (\pi/4)D$. Low energy protons, for instance the 90 keV protons responsible for the p-edge, deposit their energy in a narrow region along their paths, because secondary electrons have also small energy (approximately 200 eV at maximum for 90 keV protons) and short range (a few nanometres at maximum). For a spherical sensitive volume with an ideal isotropic response, the distribution of the path lengths is the same, irrespectively of the irradiation geometry. Conversely,

for cylindrical volumes or slab detectors, as for silicon or diamond microdosimeters, the path length distribution depends on the irradiation geometry (isotropic versus mono-directional) at least for slow ionising particles, thus the distribution of the energy imparted to the volume is more closely related to the path length, rather than to the geometrical chord length distribution. Therefore, in this work the lineal energy has been considered as the ratio between the energy imparted and the mean path length of primary tracks intersecting the sensitive volume. This quantity is more closely related to the local density of energy loss, hence to the particle LET [Solevi P. et al.., 2015; Bolst D. et al., 2017; Magrin G. 2018]. The situation is illustrated in Figure 12, which shows two cylindrical volumes, one with *H=D* and the other with *H*=4*D*, irradiated by randomly oriented tracks (corresponding to μ-randomness) or by a parallel beam. If randomly oriented tracks are considered, the mean path length is equal to the mean chord length. Consequently, the mean value of the energy imparted by a single energy-deposition event is higher in the longer cylinder, and the ratio between the mean energy imparted per single event and the mean chord length properly describes the linear density of energy deposition. If the volumes are irradiated by parallel tracks, as it is approximately the case in particle radiotherapy, then the mean energy imparted per single event is independent of the height *H* of the cylinder, because the mean path length of protons crossing the volume is independent of *H*. In this case the lineal energy as defined by ICRU 36 is not representative of the linear density of energy deposition, since the energy imparted per single event is the same for the right cylinder with *H=D* and for the longer cylinder with *H*=4*D*, but the mean chord length is greater in the second case. To get a quantity that is representative of the local density of the energy deposition we therefore considered the ratio of the energy imparted and the mean path length of protons crossing the volume.

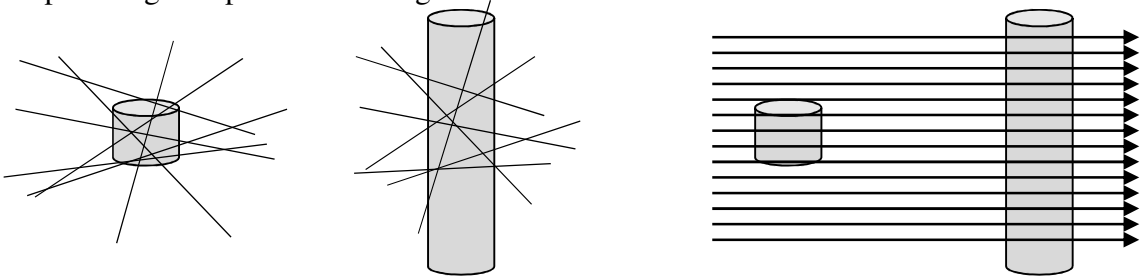

(a) *H=D*	(b) *H*=4*D*	(c) *H=D*	(d) *H*=4*D*
$\bar{l}_{\mu} = (2/3)D$	$\bar{l}_{\mu} = (8/9)D$	$\bar{l}_{\mathrm{path}} = (\pi/4)D$	$\bar{l}_{\mathrm{path}} = (\pi/4)D$

Figure 12 – Different irradiation geometries and mean chord lengths for μ-randomness (left) as compared to the mean path length for a parallel beam (right).

When measuring in a clinical proton beam as the CATANA proton SOBP, the cylindrical sensitive volume of the TEPC was irradiated orthogonally to its axis. Therefore, the probability density distribution of the intercepted track lengths, *f(l)*, depends on the diameter *D* and it is independent of the cylinder height:

$$f(l) = \begin{cases} \frac{l}{D\sqrt{D^2 - l^2}}, & 0 \le l < D \\ 0, & l \ge D \end{cases} \qquad (3)$$

The mean track length of protons crossing the cavity is the first moment of the distribution given in equation (3), $\bar{l}_{\mathrm{path}} = (\pi/4)D$. Being $D = 0.9$ mm, the mean track length for protons crossing the cylinder with parallel trajectories perpendicular to the cylinder axis is $\bar{l}_{\mathrm{path}} = 0.707$ mm.
Due to the lateral scattering of the proton beam, the actual $f(l)$ distribution may differ significantly from the simple equation (3). In order to evaluate the influence of scattered trajectories, FLUKA simulations were performed for the modulated 62 MeV proton beam beyond the Bragg peak, where the lateral scattering is maximum [G. Kraft, 2000]. Results are presented in Figure 13. The mean path-length calculated as the first moment of the simulated *f(l)* distribution equation is 0.715 mm (equivalent to 0.596 µm at density 1 g cm^{-3}).

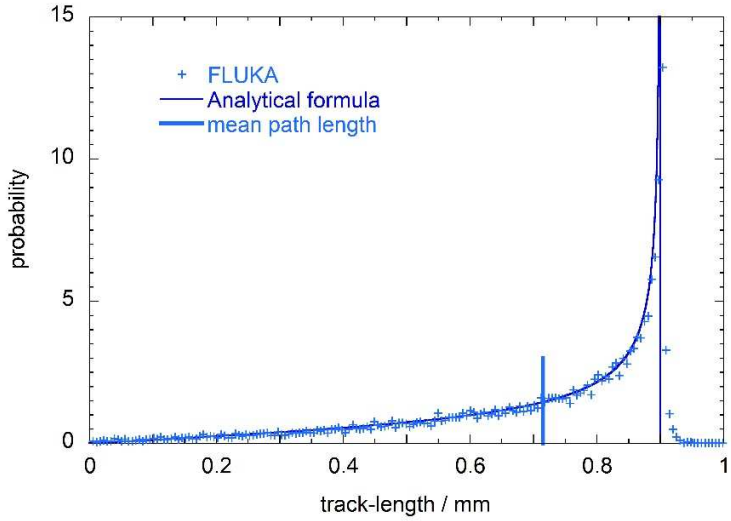

Figure 13 – Chord length distribution simulated with FLUKA for the clinical modulated 62 MeV proton beam at a depth of 30.7 mm and calculated with equation (3).

The mean path length of FLUKA was used in this paper to calculate the lineal energy in case of the clinical proton beam, while the mean chord length $\bar{l}_{\mu}$ was used for the isotropic scenario.
In this way the lineal energy values to assign to the flex position of the p-edge for a site size of 0.75 µm in propane, starting from an energy deposit value of 97 keV and depending on the irradiation geometry, are:

For the neutron field $\quad y_{\mathrm{p-edge}}^{(\mathrm{n})} = 194$ keV/µm

For the therapeutic proton beam $\quad y_{\mathrm{p-edge}}^{(\mathrm{p})} = 163$ keV/µm

3.3.3 Calibration of the e-edge

As already observed in Figure 8, the proton-edge is not always visible in proton spectra and for this reason it is useful to investigate an alternative calibration technique, for instance via the electron edge. Measurement in gamma rays radiation field were performed in the same experimental conditions as for the neutron field.

The marker in the electron-edge region is determined by following the same procedure described for the proton edge. Afterwards, a specific lineal energy value is assigned to it based on the calibration performed with the proton-edge.

Measurements and FLUKA simulations for the ^{137}Cs gamma source and the ^{7}Li(p,n)^{7}Be reaction are shown in Figure 14. Each spectrum is normalized at unit dose. The lineal energy value of the e-edge of the experimental spectrum at the flex position, based on the proton-edge calibration ($y^{(n)}_{p-edge} = 194$ keV/µm), is is $y^{(n)}_{e-edge} = 12.3$ keV/µm. The value for the e-edge found with FLUKA simulations is $y^{(\gamma)}_{e-edge}$= 11.7 keV/µm, 5% lower than the experimental value. This 5% difference is consistent with the ratio of the *W*-values for electrons and protons, which is W_{el}/W_p = 27.00 eV/28.20 eV = 0.957 [Bronic, 1997]. The experimental spectra are interpreted as energy deposition spectra, but in fact, microdosimeters measure distributions of ionizations. The number of ionizations is translated to energy deposit assuming that on average a constant energy amount is spent to produce an ion pair (*W*-value), independent of particle type and velocity. However, the mean energy spent by an electron to produce an ion pair in propane is W_{el}= 27.00 eV, slightly less than corresponding value spent by a proton, W_p = 28.20 eV. If the proper *W*-value for electrons were taken into account, the energy deposited by electrons would be reduced by a factor 0.957; therefore, the experimental lineal energy value at the e-edge would be $y^{(n)}_{e-edge} = 11.8$ keV/µm, which differs by less than 1% from the corresponding FLUKA value.

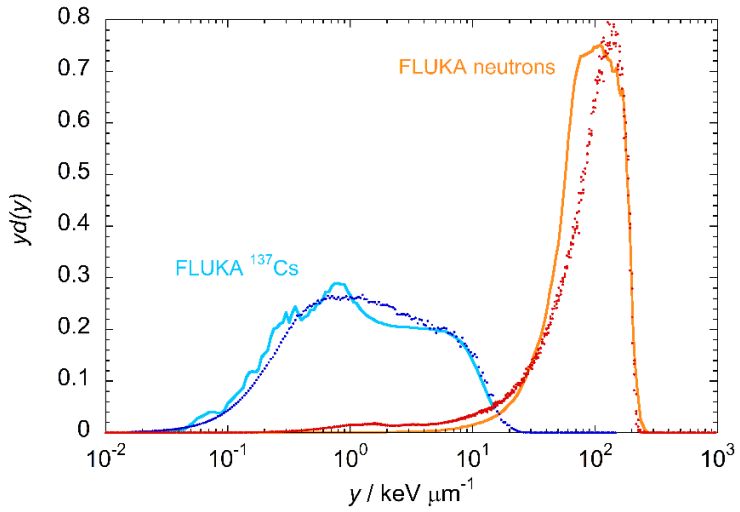

Figure 14 – Comparison between FLUKA simulated spectra (lines) and the experimental ones (dots).

A further check on the value to be assigned for calibration via the e-edge can be made using energy-range curves for electrons. The maximum energy, ε_{max}, deposited by electrons in a 0.75 µm propane site along is deposited by those electrons that have the range equal to the diameter of the site. The following equation (4) that allows finding the practical range of electrons in air [Conte, 2013] was used:

$$\frac{(R\rho)_p}{\mu g/cm^2} = 3.75 \cdot \left(\frac{T}{keV} + 0.129\right)^{1.738} - \frac{0.00059}{T/keV} + 0.0788 \qquad (4)$$

Multiplying the result by the mass stopping-power ratio $S_{\mathrm{m}}^{(\mathrm{air})}/S_{\mathrm{m}}^{(\mathrm{propane})} = 0.875$ at 10 keV according to ESTAR by NIST [Berger et al., 2017], the formula is useful to find acceptable values for practical ranges of electrons in propane. According to this procedure, the electrons that have a range of 0.75 μm in propane are those with 5.9 keV in energy. The lineal energy value to be assigned to the e-edge is obtained dividing $\varepsilon_{\mathrm{max}}$ by the mean path length for isotropic irradiation, $\bar{l}_{\mu} = 0.5$ μm, resulting in $y_{\mathrm{e-edge}}^{(\gamma)} = 11.8\ \mathrm{keV/\mu m}$, in very good agreement with the values found both experimentally and by FLUKA simulations.
Finally, if the calibration is intended for application in clinical proton beams, an additional correction for the mean path length, as discussed in Figure 14, has to be performed:

$$y_{\mathrm{e-edge}}^{(\mathrm{p})} = y_{\mathrm{e-edge}}^{(\mathrm{n})} \cdot \frac{\bar{l}_{\mu}}{\bar{l}_{\mathrm{path}}} = 12.3 \cdot \frac{0.600\ \mathrm{mm}}{0.715\ \mathrm{mm}}\ \mathrm{keV/\mu m} = 10.3\ \mathrm{keV/\mu m} \qquad (5)$$

In summary, depending on the specific application, the spectra can be calibrated using the electron edge and assigning to it the following values:

$y_{\mathrm{e-edge}}^{(\gamma)} = 11.8\ \mathrm{keV/\mu m}$	For pure gamma or x-ray spectra
$y_{\mathrm{e-edge}}^{(\mathrm{n})} = 12.3\ \mathrm{keV/\mu m}$	To calibrate neutron spectra
$y_{\mathrm{e-edge}}^{(\mathrm{p})} = 10.3\ \mathrm{keV/\mu m}$	To calibrate clinical proton beams spectra

The uncertainty associated to the calibration values are due to multiple contributions, first the determination of the marker with the fitting procedure (evaluated as less than 3%) and then the assignment of a specific lineal energy value to it, which is the main source of uncertainty. Based on the uncertainties of FLUKA simulations and the SRIM database this contribution has been evaluated as around 4%. The overall uncertainty can be estimated by the error propagation of these two contributions, obtaining a total uncertainty of 5%.

3.3.4 The calibration in water

For applications in proton therapy, where the dose and the *LET* are usually calculated in liquid water, it is of interest to calibrate the spectra in propane to lineal energy in water. To this purpose, the average stopping power ratio of propane to water was considered, in order to get the same mean energy losses from protons in water and in propane gas.
According to NIST and SRIM [Ziegler et al., 2010], the average ratio of the stopping powers of protons in water and propane for energy less than 62 MeV is approximately 0.88.
In principle, a more accurate evaluation of the water equivalent thickness should be done based on the equivalence of the ionization spectra simulated at several position along the penetration depth of the proton beam in the two materials, following the same procedure used by Chiriotti et al [Chiriotti et al., 2015]. This more detailed study will be developed in the future, while for the present work the approximation in which the ratio of the mean stopping power is used is considered

acceptable. Previous simulations of the ionization spectra in nanometre-sized volumes resulted in a ratio of equivalent site sizes of 0.8 [Grosswendt B., 2004], about 10% smaller than the factor 0.88 considered in this work.
The lineal energy values found for the proton-edge calibration in 0.75 μm in propane were directly converted into lineal energy values in water multiplying by 0.88 and obtaining:

For the neutron field $y^{(n)}_{p\text{-edge}} = 171\ \text{keV}/\mu\text{m}$

$y^{(n)}_{e\text{-edge}} = 10.8\ \text{keV}/\mu\text{m}$

For the therapeutic proton beam $y^{(p)}_{p\text{-edge}} = 143\ \text{keV}/\mu\text{m}$

$y^{(p)}_{e\text{-edge}} = 9.1\ \text{keV}/\mu\text{m}$

The overall uncertainty, obtained by the propagation of the uncertainty on the marker determination (about 3%) and the one on the lineal energy value assigned to it (about 4%), was estimated as 5%. However, the procedure is based on the use of a constant factor equal to the average of the ratio of the stopping powers of the two materials to perform the conversion from propane to water. This assumption needs to be investigated more deeply, and could imply differences larger than 5%, in particular for clinical proton beams in proximity of the Bragg peak, because for low energy protons the ratio of the mass stopping power is significantly less than the average 0.88. The differences in microdosimetric spectra simulated in propane and in liquid water will be investigated in a future work.

5. Conclusions

A calibration procedure exploiting the characteristic sharp decrease at high *y*-values present in proton or neutron spectra, known as proton-edge, has been investigated for the lineal energy calibration of microdosimetric spectra measured with a cylindrical mini-TEPC filled with pure propane gas to simulate a propane mass per area of 75 μg/cm^2. The study has been performed in the neutron field produced by the ^{7}Li(p,n)^{7}Be reaction using 2.4 MeV protons on a 100 μm thick ^{7}Li target, and at the clinical 62 MeV modulated proton beam of CATANA.
A Fermi-like function was first fitted to the proton edge region, and the precision of two markers was studied, the position of the inflection point of the fitted function, h_{flex}, and the intercept of the tangent through the inflection point with the *h*-axis, h_{tC}. In the neutron field, the overall uncertainty on h_{flex} was estimated to be 0.4%, and that on h_{tC} is 0.3%. In the clinical proton beam the uncertainties are grater, 2.5% and 3.2% respectively. Considering that h_{flex} is less sensitive to undetected variations in the gas pressure [Conte et al., 2013], this is the more adequate marker for sealed TEPCs, in which the gas density may vary over time. The uncertainty associated to the determination of h_{flex} has been estimated as smaller than 3%.
The lineal energy value to assign to h_{flex} was determined with FLUKA simulations. It was found that the maximum energy deposited by a proton in the sensitive volume, ε_{max}, is 97 keV, both for the neutron field and for the clinical proton beam. The lineal energy value at the p-edge was calculated as the ratio between ε_{max} and the mean path length of protons crossing the sensitive volume, which depends on the irradiation geometry. When the p-edge is not recognisable on the

proton spectra, a lineal energy calibration can be performed using the electron-edge in the spectrum produced by a ^{137}Cs gamma source. A good consistency of the two calibration techniques was found.
For the lineal energy calibration of microdosimetric spectra in 0.75 um of propane the following values were found:

$y_{\text{p-edge}}^{(\text{n})} = 194\ \text{keV}/\mu\text{m}$ and $y_{\text{e-edge}}^{(\text{n})} = 12.3\ \text{keV}/\mu\text{m}$ in neutron field and
$y_{\text{p-edge}}^{(\text{p})} = 163\ \text{keV}/\mu\text{m}$ and $y_{\text{e-edge}}^{(\text{p})} = 10.3\ \text{keV}/\mu\text{m}$ in clinical proton beams

The lineal energy calibration in water can be obtained by using the average ratio between the stopping powers of protons in water and propane, which is about 0.88 according to NIST and SRIM:

$y_{\text{p-edge}}^{(\text{n})} = 171\ \text{keV}/\mu\text{m}$ and $y_{\text{e-edge}}^{(\text{n})} = 10.8\ \text{keV}/\mu\text{m}$ in neutron field and
$y_{\text{p-edge}}^{(\text{p})} = 143\ \text{keV}/\mu\text{m}$ and $y_{\text{e-edge}}^{(\text{p})} = 9.1\ \text{keV}/\mu\text{m}$ in clinical proton beams

Alternative databases other than those implemented in FLUKA can be used to calculate the maximum energy imparted by protons to the sensitive volume. The selection of different database contributes for a difference of about 4% in propane [Chiriotti et al., 2015b], by propagating the uncertainties on the marker determination (3%) and the lineal energy value to ascribe to it in propane (4%) an overall uncertainty of 5% is found.
The uncertainty on the calculation of the imparted energy is a systematic error, as it causes a rigid shift to higher or lower lineal energy values. With this respect, when presenting microdosimetric spectra it is recommended to specify which database (ICRU, FLUKA, SRIM etc.) is used to calculate the $y_{\text{p-edge}}$, or alternatively to declare which marker has been selected for calibration purposes and which lineal energy value has been assigned to it. A strategy to reduce the uncertainty on the calculation of the calibration factor can be to use and compare different calibration techniques (for instance using a set of mono-energetic particle beams of known energies).
It should be observed that an accurate calibration at the proton-edge does not immediately imply *per se* that the shape of the spectra is also accurate. The response function of the detector (due to measuring principle, shape, material composition etc.) can influence the shape of the spectrum.
In particular, potential differences between the ionization and the energy imparted spectra, describing different random processes, will be investigated in a future work based on Monte Carlo simulations.
Similarly, the differences between the distributions of energy imparted to the mini-TEPC gas cavity and to a sensitive volume made of liquid water will also be studied by means of Monte Carlo simulations.

Acknowledgements

This work was supported by the 5th Scientific Commission of the Italian Institute for Nuclear Physics (INFN), the Belgian Nuclear Research Centre SCK CEN and Hasselt University.
This work has been partially supported by the ENEN+ project that has received funding from the EURATOM research and training Work Programme 2016 – 2017 – 1 #755576.

References

- Berger M. J., et al., National Institute of Standards and Technologies (NIST) Standard Reference Database 124, *Stopping-power and range tables for Electrons, Protons and Helium ions database,* (2017).
- Bianchi et al., Radiat. Phys. Chem., *Microdosimetry with a sealed mini-TEPC and a silicon telescope at a clinical proton SOBP of CATANA*, (2020) 171, 108730.
- Bronic I. K., Rad. Prot. Dosim., *W values in propane-based tissue-equivalent gas*, (1997) 70, 33-36.
- Böhlen T.T. et al., Nuclear Data Sheets *The FLUKA Code: Developments and Challenges for High Energy and Medical Applications*, (2014) 120, 211-214.
- Bolst D. et al., Phys. Med. Biol. *Correction factors to convert microdosimetry measurements in silicon to tissue in 12C ion therapy,* (2017) 62(6), 2055-2069.
- Cirrone G.A. P., et al., IEEE Trans. Nucl. Sci., *A 62-MeV proton beam for the treatment of ocular melanoma at Laboratori Nazionali del Sud-INFN,* (2004) 51 (3), 860‑865.
- Chiriotti S., et al., Radiat. Protect. Dosim., *Equivalence of pure propane and propane TE gases for microdosimetric measurements*, (2015) 166 (1-4), 242–246.
- Chiriotti S. et al., Radiat. Protect. Dosim., *Influence of the physical data to calibrate TEPCs*, (2015b) 166 (1-4), 238-241.
- Conte V. et al., Multidisciplinary Applications of Nuclear Physics with Ion Beams (ION BEAMS ’12) – AIP Conf Proc, *Linear energy calibration of mini tissue equivalent gas-proportional counters (TEPC)*, (2013) 1530, 171-178.
- Conte V. et al., Phys. Med., *Microdosimetry at the CATANA 62 MeV proton beam with a sealed miniaturized TEPC* (2019) 62, 114-122.
- De Nardo L. et al., Radiat. Protect. Dosim., *Mini-TEPCs for radiation therapy.* (2004) 108 (4), 345‑352.
- Ferrari A. et al., CERN-2005-10, INFN/TC_05/11, SLAC-R-773, *FLUKA: a multi-particle transport code (2005)*
- Grosswendt B., Radiat. Prot. Dosim. *Recent advances of nanodosimetry* (2004) 110, 789-99.
- International Commission on Radiation Units and Measurements (ICRU), *Microdosimetry. Report 36* (1983).
- International Commission on Radiation Units and Measurements (ICRU), *Stopping powers and ranges for protons and alpha particles. Report 49* (1993).
- International Commission on Radiation Units and Measurements (ICRU), *Fundamental quantities and units for ionizing radiation. Report 85* (2011).
- Kraft G., Progress in Particle and Nuclear Physics *Tumor therapy with heavy charged particles* (2000) 45, S473-S544.
- Lindborg et al., CRC Press, *Microdosimetry : experimental methods and applications,* (2017), 204 p.

- Magrin G., Phys. Med. Biol. *A method to convert spectra from slab microdosimeters in therapeutic ion-beams to the spectra referring to microdosimeters of different shapes and material* (2018) 63:215021.
- Mazzucconi D. et al., Radiat. Meas., *Monte Carlo simulation of a new mini-TEPC for microdosimetry at nanometric level: Response against a carbon ion beam,* (2018) 113, 7-13.
- Menzel, H.G., et al., Int. J. Radiat. Biol. *Microdosimetric specification of radiation quality in neutron radiation therapy*, (1990) 57, 865–883.
- Solevi P. et al., Phys. Med. Biol. *Monte Carlo study of microdosimetric diamond detectors* (2015) 60, 7069.
- Wambersie A. et al., Radiat. Protect. Dosim., *The role of microdosimetry in radiotherapy*. (1990) 31, 421–432
- Ziegler J.F. et al., Nucl. Instr. Meth., *SRIM The stopping and range of ions in matter*, (2010) B 268, 1818–1823.